# INVERSION OF ELECTROMAGNETIC DATA FOR HYDRAULIC FRACTURE DIAGNOSTICS IN OPEN-HOLE WELLS

**J.F. SHIRIYEV,**
Doctor of Technical Sciences
in Oil and Gas Reservoir
Development, Docent at Baku
Higher Oil School,
*cavid.shiriyev@bhos.edu.az*

**K.S. MAMMADOV,**
PhD student in Oil and
Gas Reservoir Exploitation,
Lecturer at Baku Higher
Oil School,
*kanan.mammadov@bhos.
edu.az*

BAKU HIGHER OIL SCHOOL
Azerbaijan Republic, Baku, Bibi-Heybat Campus

*A simulated-annealing-based inversion algorithm was developed for processing tri-axial induction data to estimate the geometry and conductivity of hydraulic fractures. This method successfully provides accurate estimates of fracture length, conductivity, and dip angle. By using a mono-axial transmitter and tri-axial receiver coils with co-axial and cross-polarized configurations, the fracture properties, including geometry and conductivity, are effectively recovered. For circular fractures, the conductivity and radius are accurately estimated, while elliptical fractures result in recovery of an equivalent circular radius. Variations in proppant concentration are reflected in the inverted conductivity, approximating the average conductivity across the fracture. The tool demonstrates sensitivity to fracture dip angle, with accurate estimates even in heterogeneous rock formations, provided that signals from fractured and non-fractured states are properly subtracted.*

*The tool's current configuration is capable of detecting conductive fractures up to 40 meters in radius, with the accuracy of results improving through enhanced receiver sensitivity and increased tool spacing. The study also reveals that neighboring fractures can influence inversion accuracy, especially at closer spacing. A multi-fracture inversion strategy is proposed for efficient processing, ensuring that multiple fractures can be accurately modeled in the inversion process without affecting the final results. These findings suggest that electromagnetic induction logging, when appropriately configured, holds great promise for real-time monitoring and diagnosing hydraulic fractures in field conditions.*

# АШЫҚ ҰҢҒЫМАЛАРДАҒЫ ГИДРАВЛИКАЛЫҚ ЖАРЫҚШАҚТАРДЫ ДИАГНОСТИКАЛАУ ҮШІН ЭЛЕКТРОМАГНИТТІК ДЕРЕКТЕРДІ ИНВЕРСИЯЛАУ

**ДЖ.Ф. ШИРИЕВ,** техникалық ғылымдар докторы, мұнай және газ кен орындарын игеру маманы, доцент, Баку Жоғары Мұнай Мектебі, *cavid.shiriyev@bhos.edu.az*
**К.С. МАМЕДОВ,** мұнай және газ кен орындарын игеру мамандығы бойынша аспирант, оқытушы, Баку Жоғары Мұнай Мектебі, *kanan.mammadov@bhos.edu.az*

БАКУ ЖОҒАРЫ МҰНАЙ МЕКТЕБІ
Әзербайжан Республикасы, Баку, Биби-Эйбат кампусы

*Симуляциялық күйдіру негізінде инверсия алгоритмі гидравликалық жарылыстардың геометриясы мен өткізгіштігін бағалау үшін үш осьті индукция деректерін өңдеу үшін әзірленді. Бұл әдіс жарылыс ұзындығы, өткізгіштігі және еңкейту бұрышының дәл бағаларын қамтамасыз етеді. Моноосьті таратқыш катушка және үш осьті қабылдаушы катушкалармен, коаксиалды және крест тәрізді конфигурацияларда жарылыс қасиеттері, оның ішінде геометриясы мен өткізгіштігі, тиімді түрде қалпына келтіріледі. Дөңгелек жарылыстар үшін өткізгіштік пен радиус дәл бағаланады, ал эллиптикалық жарылыстар үшін эквивалентті дөңгелек радиус қалпына келтіріледі. Пропан концентраттарының өзгерістері инверттелген өткізгіштікте, жарылыс бойындағы орташа өткізгіштікке жақындайды. Құрал жарылыс еңкейту бұрышына сезімталдықты көрсетеді, тіпті гетерогенді жыныс қорларында да дәл бағалаулар береді, егер жарылыссыз және жарылысты жағдайлардан алынған сигналдар дұрыс шегерілсе.*

*Құралдың қазіргі конфигурациясы 40 метр радиусына дейінгі өткізгіш жарылыстарды анықтай алады, нәтижелердің дәлдігі қабылдағыштардың сезімталдығын арттыру және құралдың арақашықтығын ұлғайту арқылы жақсарады. Зерттеу сондай-ақ көрші жарылыстар инверсия дәлдігіне әсер етуі мүмкін екендігін көрсетеді, әсіресе жақын орналасқан жағдайда. Көпжарылысты инверсия стратегиясы тиімді өңдеу үшін ұсынылады, бұл бірнеше жарылысты инверсия процесінде дәл модельдеуге мүмкіндік береді, нәтижелерге әсер етпей. Осы нәтижелер көрсеткендей, электромагниттік индукция логгингін дұрыс конфигурациялау кезінде гидравликалық жарылыстарды нақты уақыт режимінде мониторингтеу және диагностикалау үшін үлкен әлеуетке ие.*

*ТҮЙІН СӨЗДЕР: гидравликалық жарықшақ, үш осьті электромагниттік индукциялық каротаж құралдары, нақты уақыттағы мониторинг, имитациялық шынықтыру, жарықшақ геометриясының параметрлері, жарықшақ еңкіштігі, көршілес жарықшақтар, бірнеше кластерге арналған инверсиялық стратегия, толтырғышты бөлу, жару кезеңі, төмен жиілікті индукциялық құрал.*

# ИНВЕРСИЯ ЭЛЕКТРОМАГНИТНЫХ ДАННЫХ ДЛЯ ДИАГНОСТИКИ ГИДРАВЛИЧЕСКИХ РАЗРЫВОВ В ОТКРЫТЫХ СКВАЖИНАХ

**ДЖ.Ф. ШИРИЕВ,** доктор технических наук по разработке нефтегазовых месторождений, доцент Бакинской Высшей Нефтяной Школы, *cavid.shiriyev@bhos.edu.az*
**К.С. МАМЕДОВ,** аспирант по эксплуатации нефтегазовых месторождений, преподаватель Бакинской Высшей Нефтяной Школы, *kanan.mammadov@bhos.edu.az*

БАКИНСКАЯ ВЫСШАЯ НЕФТЯНАЯ ШКОЛА
Республика Азербайджан, Баку, кампус Биби-Эйбат

*Был разработан инверсионный алгоритм, основанный на методе имитационного отжига для обработки данных триосевой индукции с целью оценки геометрии и проводимости гидравлических трещин. Этот метод успешно предоставляет точные оценки длины трещин, проводимости и угла наклона. С использованием моноосевой передающей катушки и триосевых приемных катушек с коаксиальными и крестовыми конфигурациями, свойства трещин, включая геометрию и проводимость, эффективно восстанавливаются. Для круглых трещин проводимость и радиус оцениваются точно, в то время как для эллиптических трещин восстанавливается эквивалентный круглый радиус. Изменения в концентрации проппанта отражаются в инвертированной проводимости, приближаясь к средней проводимости по всей трещине. Инструмент демонстрирует чувствительность к углу наклона трещины с точными оценками даже в гетерогенных горных породах при условии правильного вычитания сигналов из состояния с трещинами и без.*

*Текущая конфигурация инструмента способна обнаруживать проводящие трещины радиусом до 40 метров, при этом точность результатов улучшается с повышением чувствительности приемников и увеличением расстояния между инструментами. Исследование также показывает, что соседние трещины могут влиять на точность инверсии, особенно при меньшем расстоянии. Предлагается стратегия многотрещинной инверсии для эффективной обработки, которая обеспечивает точное моделирование нескольких трещин в процессе инверсии без влияния на конечные результаты. Эти результаты показывают, что электромагнитный индукционный логгинг при правильной настройке имеет большой потенциал для реального мониторинга и диагностики гидравлических трещин в условиях эксплуатации.*

*КЛЮЧЕВЫЕ СЛОВА: гидравлический разрыв, трехосные электромагнитные индукционные каротажные инструменты, мониторинг в реальном времени, имитация отжига, параметры геометрии разрыва, угол наклона разрыва, соседние разрывы, стратегия инверсии для нескольких кластеров, распределение наполнителя, стадия разрыва, низкочастотный индукционный инструмент.*

**Introduction.** A combination of hydraulic fracturing treatments with horizontal drilling has led to a breakthrough in hydrocarbon production by enabling hydrocarbon recovery from low permeability shale rocks. While the unpropped portions of induced fractures close under high net stress shortly after fracturing, it is the proppant filled fracture that contributes to the well productivity (Sharma and Manchanda, 2015). Therefore, fracture monitoring techniques should be deployed to monitor, appraise and quantify the geometry of such propped fractures.

Conventional fracture diagnostic techniques, such as microseismic monitoring and tiltmeter mapping, are based on sensing physical events that occur during fracture growth.

These techniques are not suitable for deducing the proppant distribution in fractures due to the lack of correlation between the detected activity and proppant location. More recent fiber optic-based measurements provide data that can be qualitatively interpreted for the efficiency of proppant placement. The temperature based monitoring (DTS) lacks the same correlation with proppant location, and in some applications, combined temperature and acoustic (DAS) sensing have been used to infer dominant perforation clusters containing most of the fracturing fluid and proppant (Sookprasong et al., 2014; Wheaton et al., 2016).

A more promising alternative for proppant detection is to use techniques that rely on sensing electromagnetic (EM) fields scattered due to the contrast in EM material properties between the propped fractures and the surrounding formation. Numerous proppant types are reported to exhibit large effective electrical conductivities in LaBrecque et al. (2016), Palisch et al. (2016), Zhang (2018) and Hoversten et al. (2015). They can be used for such an application along with a variety of field data acquisition techniques to sense the EM fields scattered from proppants. A tri-axial electromagnetic induction logging tool is one of these techniques that utilizes downhole sources and receivers in the vicinity of propped hydraulic fractures which enables improved spatial resolution of the fracture properties. It has the potential to offer a far-field proppant detection technique that can be executed from a single wellbore at any time during the well's life cycle. Therefore, the method can provide time-lapse analysis of fracture growth or closure, which can decrease the uncertainties in reservoir parameters critical for long-term production forecasting (Balan et al., 2017). Furthermore, the application of such measurements in the field can be incorporated with complex-fracture proppant transport models (Blyton et al., 2015; Shrivastava and Sharma, 2018) to improve their reliability.

Basu and Sharma (2014), Zhang et al. (2016), Dai et al. (2018) and Shiriyev et al. (2018) studied such a low frequency induction tool (*Figure 1*) numerically and experimentally and found it to be sensitive to various propped fracture properties in open-hole well completions. It includes a mono-axial transmitter coil that generates EM fields and two tri-axial receiver coil sets (short and long spacing) recording the EM response of the surrounding formation. The second receiver (bucking) coil in each set is used to approximately cancel the dominant imaginary component of the primary field and to detect signals only associated with fields arising due to the presence of a fracture filled with an electrically conductive proppant. An actual measurement in the field involves two passes of the tool along the wellbore, before and after the hydraulic fracturing, and the difference between these two bucked signals is referred as the "differential signal" (Shiriyev et al., 2018).
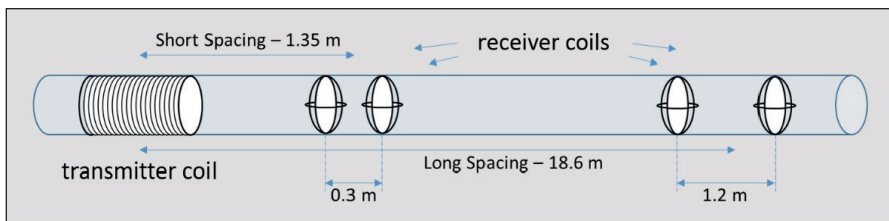


Short Spacing – 1.35 m   receiver coils

transmitter coil

0.3 m   Long Spacing – 18.6 m   1.2 m

*Figure 1* – **An electromagnetic induction logging tool with nominal spacing for short- and long-distance transmitter-receiver couples**

After logging the well with the induction tool, information on the proppant distribution in the fracture can be extracted in two different ways. The more practical and computationally less intensive approach is the parametrization of fractures. Yang et al. (2016) used circular/elliptical fractures to characterize the hydraulic fractures and utilized parametric inversion technique where the model parameters are evaluated independently in each iteration. This technique leads to a small number of model parameters, increasing computation efficiency. The other approach is the generation of a conductivity map, which provides information about the secondary fracture branches. In this case, one challenge is the computational time required for the 3D volumetric solution of Maxwell's equations. The other challenge is the solution of the inherently under-determined problem where the number of model parameters will be dependent on the resolution requirements. In this paper, we have selected the first approach, and we apply a stochastic inversion technique, which is based on a simulated-annealing method, to estimate the hydraulic fracture properties. The inversion model is fully automated, fast and robust.

The paper first discusses open-hole simulation of electromagnetic signals as the forward model used in the inversion algorithm. Following the forward model, the inversion methodology is described, and it is tested on a synthetic data set to evaluate the sensitivity of the signals to fracture electrical conductivity, size and dip-angle. The model was further used to evaluate the area of investigation of the tool with the given optimized frequency and tool spacing. Finally, we study the effect of neighboring fractures on the recorded signals to accurately identify proppant distribution among many fractures in a stage. The results and conclusions of the paper enable the design and interpretation of data from a field deployable tool.

**Electromagnetic Forward Modeling.** While logging a well with the induction tool, the tool is pulled along the wellbore, and the transmitter coil is excited at certain sampling points requiring the forward model to calculate signals for each one. Therefore, a frequency domain computation is ideal for the analyses where the system matrix obtained after deploying a numerical technique is usually independent of changing sampling points. Once this matrix is inverted or factorized, it can be used to obtain solutions for all excitations providing significant computational advantages.

Maxwell's equations in the frequency domain can be solved using one of several numerical methods. In this paper, we have utilized two numerical approaches. In the first approach, the system is solved with a method of moments (MOM; Rao et al., 1982). Since the thickness of fractures is much smaller than their length and skin depth, we can make the assumption of a zero thickness surface for the fracture models, rather than a very thin volume (Zhang et al., 2016) facilitating the use of surface integral equations (Qian et al., 2007) with the MOM. This approach is especially well suited for our analysis because it confines the computational domain to the anomalous conductivity region only and allows simulation of all fracture parameters listed in Yang et al. (2015; 2016; 2017): fracture location, conductivity, size, shape factor and dip-angle.

The second numerical approach uses the assumption of axial symmetry to avoid an outrageous increase in the number of unknowns when the simulation of heterogeneous background conductivity is required (Zhang et al., 1999; Wang et al., 2009; Pardo and Torres-Verdin, 2013). In cylindrical coordinates, the ϕ-direction of the problem can be

eliminated by using a Fourier series, and the set of 2D problems can be solved with different types of numerical solvers. The axial hybrid method is used to solve the reduced 2D problem where the numerical solution is obtained in the wellbore direction, and a family of normalized Bessel functions is used to describe the EM fields in the radial direction (Gianzero et al., 1985; Pai, 1991; Li and Shen, 1993). In this approach, however, we lose the capability of simulating the fracture parameters such as shape factor and dip-angle. The details of the forward model calculation are provided in Shiriyev (2018).

**Inversion Method.** The short spacing receiver coil (*Figure 1*) can detect smaller fractures but is insensitive to larger ones, and the long spacing responds to larger fractures, although the signal is much weaker. To equalize their weight in the overall objective function, all the relative errors are calculated as below:

$$E_{uv} = \sum_i \left( \frac{\Delta U_{uv}^i - \Delta \widetilde{U}_{uv}^i}{\Delta \widetilde{U}_{uv}^i} \right)^2 \tag{1}$$

where $\Delta U$ is the differential signal; subscripts $u$ and $v$ denote the orientation of receiver and transmitter coil, respectively; $i$ is the index of sampling point; and the tilde refers to the measured (true or observed) data. For all our presentations here, "calculated data" (w/o tilde) is computed using coarser surface meshes generated based on the new iteration parameters. For the "measured data" (with tilde), finer surface mesh is used with an additional one percent of random noise. We have also avoided running the same simulator for the measured and calculated data in cases such as symmetrical and orthogonal fractures. Finally, in all calculations, the differential signals are above the threshold values when calculated with practical coil moments (Shiriyev, 2018).

The use of a tri-axial receiver coil system allows the recovery of more fracture parameters. In the previous numerical study (Yang et al., 2016), co-axial measurements were shown to be sensitive to the fracture cross-sectional area but cannot differentiate fractures of the same area with different cross-sectional shapes or dips. The co-polarized measurements can discern axially symmetric from asymmetric fractures but are found to be weak (Shiriyev et al. 2018), and therefore, excluded in the inversion analysis. The cross-polarized measurements can quantify fracture dip-angle and become more pronounced as the dip-angle increases. For an accurate estimation of all model parameters, we define the overall objective function in such a way that it includes all the signals from different coil spacings and configurations:

$$E = \left( E_{zz} + E_{yz} \right)^{\text{short}} + \left( E_{zz} + E_{yz} \right)^{\text{long}}, \tag{2}$$

zz is the co-axial configuration and *yz* is one of the cross-polarized configurations. This cost function combines all four signals effectively and enables a global search on the fracture parameters, which is described next, as opposed to parametric search suggested in Yang et al (2016).

**Derivative free directional search technique.** Typically, stochastic inversion techniques randomly select a starting point in the model space and moves are decided based on control parameters. Simulated-annealing (Fouskakis and Draper, 2002; Sen and Stoffa, 2013) uses temperature as a control parameter for accepting or rejecting a selected model and for calculating the jump distance and direction at each iteration. In this study,

we start the iteration with multiple models, and the tuning parameters are 1) the cooling schedule, 2) the number of models in an ensemble and 3) the number of iterations.

The main goal of the inversion algorithm is to minimize the error calculated using Eq. 2, and the work flow is outlined in *Figure 2*. First, we define the limits for each individual model parameter. The lower bound is defined as **m**$^{min}$ and upper bound as **m**$^{max}$. Then the first ensemble of models is randomly generated as follows:

$$\mathbf{m^1} = \mathbf{m}^{min} + r_u \cdot (\mathbf{m}^{max} - \mathbf{m}^{min}), \tag{3}$$

where $r_u$ is the random number generated from the uniform distribution. Errors for the models are then evaluated, and the selection is carried to replace the selected number of worst models with the best model. At the end of each iteration, new models are generated from the old ones as follows:

$$m_i^{new} = m_i^{old} \mp r_u \cdot T \cdot \Delta m_i, \tag{4}$$

where $i$ is the index number of the model in the ensemble and $T$ is the control temperature which gradually decreases by the iterations according to one of the predefined schedules shown in *Figure 3* (Fouskakis and Draper, 2002). The cooling schedule allows larger jumps at the beginning of the search and smaller jumps toward the end of the search. Generally, a faster cooling schedule may cause the solution to be stuck in a local minimum. A slower cooling schedule is more likely to find a global minimum at the cost of an increase in the computation time.
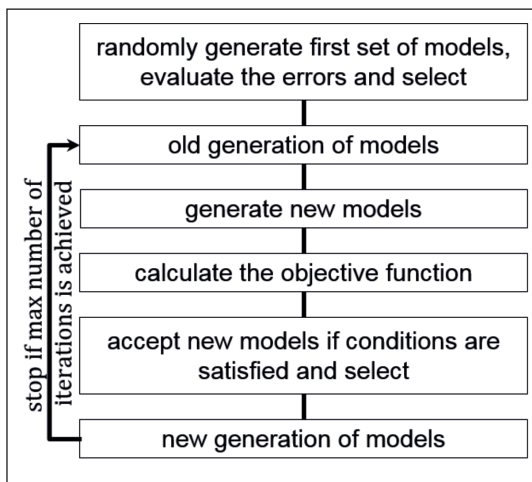


*Figure 2* – **Flow diagram of simulated-annealing based inversion algorithm**

The models in previous and new iterations are compared pairwise as follows:

$$E(m_i^{new}) \leq E(m_i^{old}) \quad \text{or} \quad T > r_u, \tag{5}$$

here, the temperature ($T$) is used to decide whether to keep a larger error model or not. At the beginning of the search, we have a higher chance of accepting new models with larger errors which decreases almost to zero toward the end of the search. After obtaining a new set of models, the same selection procedure is applied. Finally, the algorithm is terminated when the maximum number of iterations is achieved. The ensemble-based

method used here avoids rejection of a large number of trial models as used in the conventional simulated-annealing and thus converges in fewer iterations.
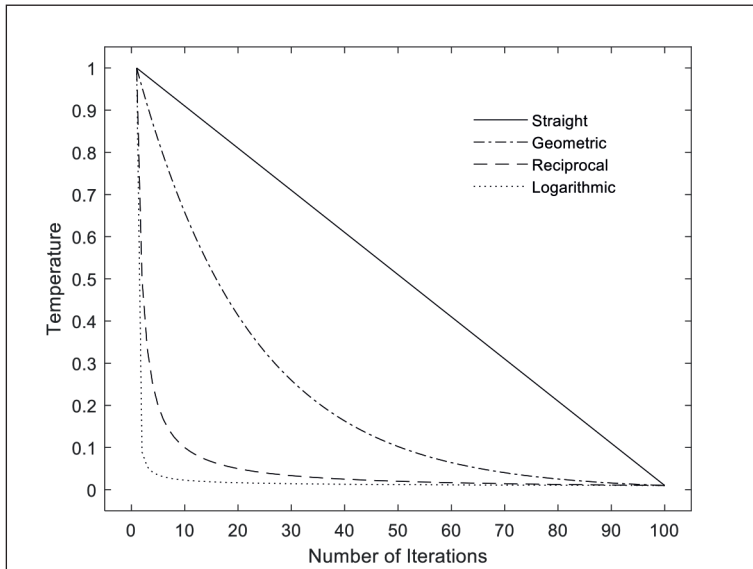


*Figure 3* – **Temperature schedules used in simulated annealing**

**Results**. We first apply the proposed algorithm to single fracture models, and then an inversion strategy is proposed for use in the presence of multiple fractures. For all results, the number of iterations is 100, the number of models in the ensemble is 5, which makes 500 total forward model runs, and the number of model parameters is either 2 or 3 depending on the fracture under consideration (to avoid zero division in Eq. 1). The first two model parameters are fracture conductivity and radius. The range for fracture conductivity is selected to be 1-500 S/m, and it is 1-50 m for the fracture radius. If the observed data has significant signal levels on the cross-polarized configuration, the model parameters include another parameter – dip-angle as well where the selected range is 0-80˚. A geometric temperature schedule was found to be the optimum temperature profile for this problem, and in the selection, the two worst models are replaced with the best model. In runs, meshes are coarsened to decrease the computation time. Typical single- and multi-cluster analyses take 10 minutes and 10 hours, respectively.

**Single cluster analysis.** The results for a single fracture inversion are shown in Figure 4. The first row shows the "true" results for circular-orthogonal (I), circular-rotated (II), elliptical (III) and variable conductivity (IV) fractures. The first three models have a constant conductivity on the entire face of the fracture, and the last model has radially and linearly decreasing conductivity toward the fracture tip. The second row in the figure shows the box plots with the statistical information for the fifty lowest error models. In each box, the central mark indicates the median, and the bottom and top edges of the box indicate the 25th and 75th percentiles, respectively. The whiskers extend to the lower and upper adjacent values, and outliers are shown with the '+' symbol. In circular (I) and

rotated (II) fractures, the whiskers of both box plots cover the interval very close to the true parameters. In the elliptic fracture (III), the results for conductivity shows the same success. For the box plot of fracture radius, however, results converged to the effective radius (which is defined as the square root of the product of major and minor radii). In the variable conductivity fracture (IV), the whiskers of box plots cover the interval, which includes the effective parameters. The third row shows error values calculated at the given iteration number for the different realizations, and for all cases, errors show a decreasing trend with the number of iterations. Finally, the last row shows calculated best models with the least error.

To see the effect of rotation in the inversion of elliptical and variable conductivity fractures, we run Models III and IV with 30° dip-angle rotated about the vertical axis. For the size and conductivity, we obtained the same results as in *Figure 4*, and the dip angle with the lowest error was in 30.2° and 29.0°, respectively.
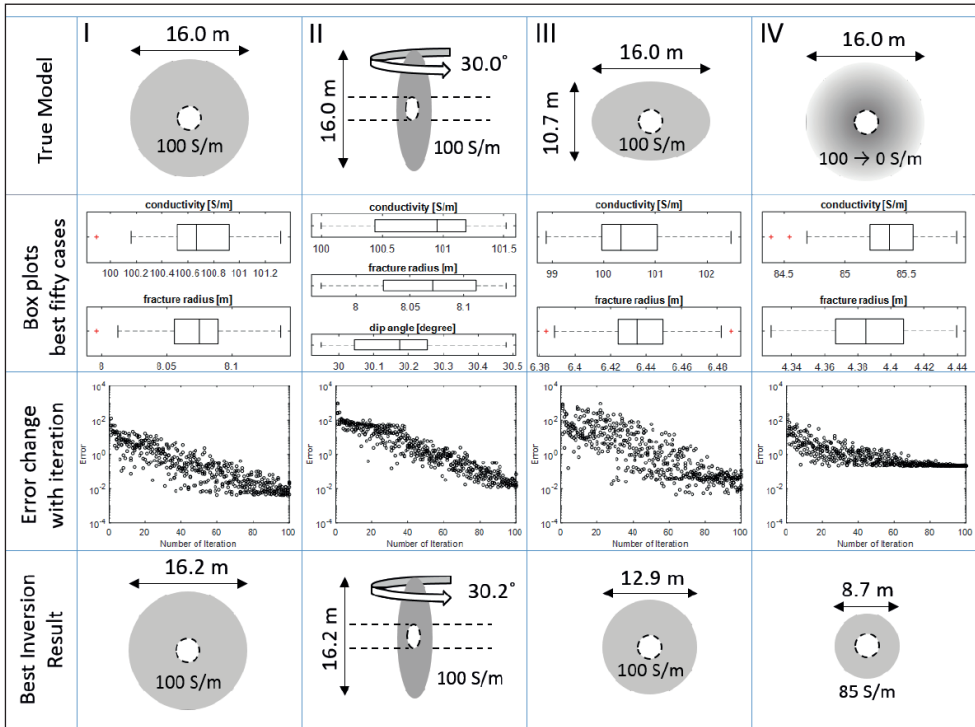


Figure 4 – **Inversion results for a single fracture**

The above results were for a homogeneous background (rock) conductivity. Now, the circular model (I) is simulated in a heterogeneous formation using the axial hybrid method and the gridding scheme is shown in *Figure 5*. The uniform region of the mesh is selected between -1 and 1 m with 10 cm intervals. The computation domain is truncated at 156 m on both sides with the grid size ratio of 1.25 in the expanding region. At every grid, in each of the three layers, we use a randomly selected conductivity between 0 and 1 S/m where the overall mean conductivity is 0.49 S/m which is the value used in the inversion runs. We get the same level of accuracy as in Figure 4, only if we subtract the

before and after fracturing signals accurately. If we repeat the same analysis without the subtraction, the accuracy is very poor; for Model I we obtain a diameter of 4 m and a conductivity of 150 S/m. This highlights the importance of making measurements both before and after fracturing.
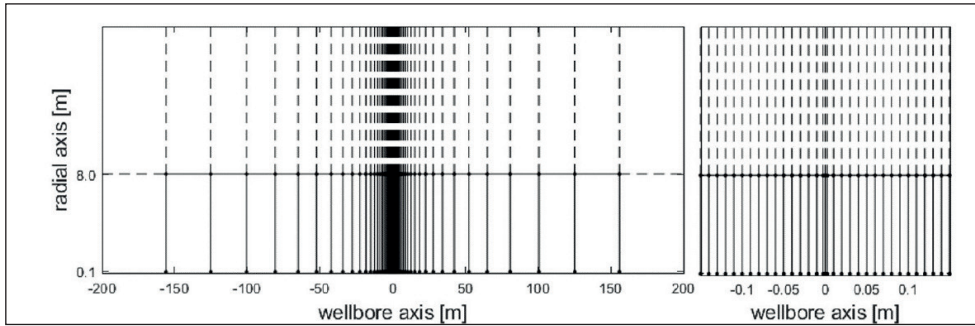


*Figure 5 –* **Meshing and radial layering scheme used in the axial hybrid method; right figure shows closer view to the fracture located region**

**Depth of investigation.** To estimate the area of investigation of the tool, we run multiple realizations by increasing the radius of fractures and calculating a variation in the inverted fracture parameters. *Figure 6* shows results for the tool with nominal spacings and properties, and there are at least five different realizations for a given radius of a fracture. A hundred of the most successful results are shown in the box plots. The measured variation is calculated by subtracting the true model parameter from the calculated value. In the runs, the fracture conductivity for the true model is 100 S/m.

The results show that once the radius surpasses 40 m, the tool with our chosen spacing and properties loses resolution. It is important to mention that this finding agrees with Yang et al. (2016) results. The variation of fracture conductivity, however, is not increasing for this uniformly distributed conductivity case. To determine fracture sizes larger than 40 m we can use a longer spacing for the tool but we need to make sure that signals are detectable. One way to increase these signal levels is to deploy transmitter and receiver coils with a higher magnetic dipole moment.
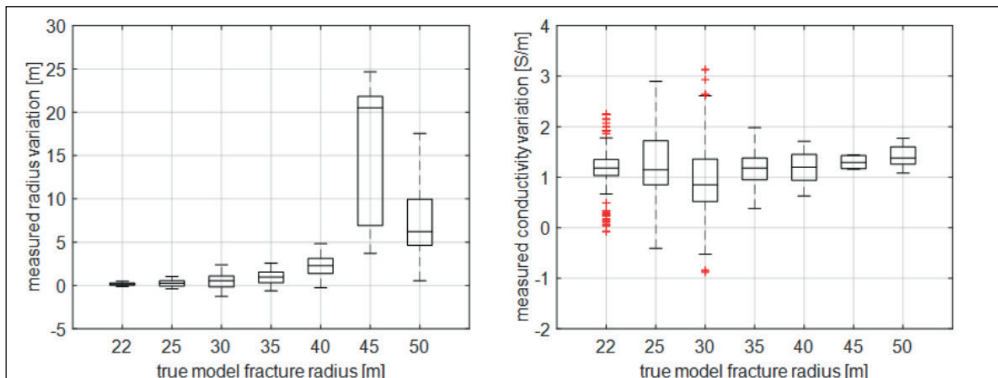


*Figure 6 –* **Box plots for the inverted results vs. actual fracture radius: calculated variation of fracture radius (left) and fracture conductivity (right). The boxes include 100 of the lowest error results from 5 different realizations**

**Multi-Cluster Inversion.** In a typical hydraulic fracturing operation, there are more than 20 stages and every stage includes 3 to 10 perforation clusters. Each of these fractures will affect the signals received by the tool. To evaluate this effect, we run many cases varying the number of fractures near the main fracture under consideration. Then, we implement a multi-fracture inversion approach to get the distribution of proppant in each fracture accurately.

*Figure 7* shows in-phase signals for short (upper figure) and long (lower figure) spacing configurations in three different cases (a, b and c). In all of the cases, the distance between clusters is selected to be 9 m (~30 ft.) and the radius of the fractures is 10 m. The number of fractures in the neighborhood of the fracture of interest (located at 0 m) are 1, 2 and 3 for cases a, b and c, respectively. In the short spacing receiver, we do not see any significant effect of the neighboring fractures. In the long spacing receiver, however, the two closest neighbors are interfering with the signal of interest. The cases with two and three neighbors give almost the same signals around the fracture of interest. Hence, in the multi-fracture inversion, we include the effect of only the closest two neighboring fractures in the multi-fracture inversion to minimize the computation time.
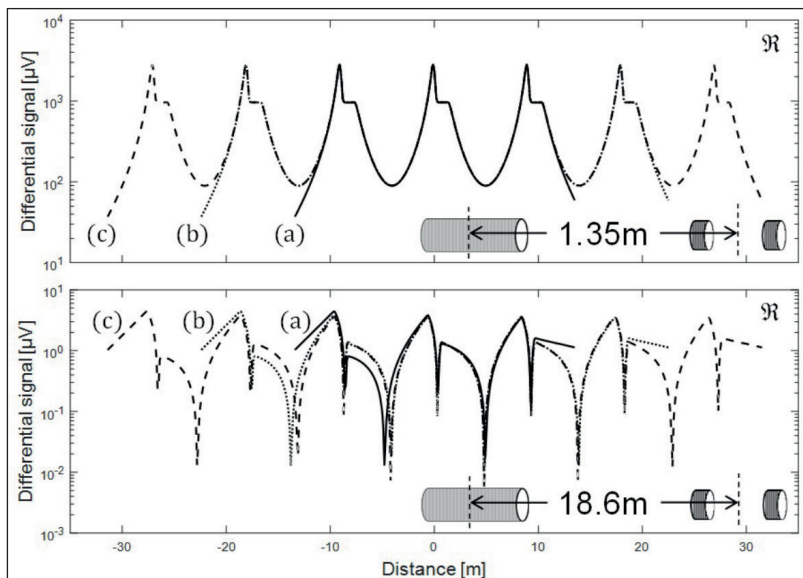


*Figure 7 –* **The effect of neighbors on the differential signals recorded in short (upper) and long (lower) coil spacings. Plots show differential signals for one (a), two (b) and three (c) neighbors on both sides of the middle fracture**

The technique used for the inversion is to first invert the data for each fracture assuming that it has no neighbors. Then, these results are used as initial guesses for the neighbors in multi-fracture inversion. In this second iterative step, we include the two closest neighbor fractures on both sides of the fracture of interest (maximum of five total fractures in each forward model). To demonstrate this procedure, we use two cases shown in *Figure 8*.

In *Figure 8*, the first column shows "true" models for the two cases. Then, for each fracture, we invert the signals in the interval of (-1, 1) m and show the best results for the single fracture inversion in the second column. The best models after two sets of iterations are shown

in the third column. In Case 1, we are using two model parameters, fracture conductivity and size. In Case 2, we use three model parameters (conductivity, size and dip-angle) for the third and fourth fractures (from left) and two parameters (conductivity and size) for the rest. The calculated multi-fracture inversion results are in good agreement with the true models.
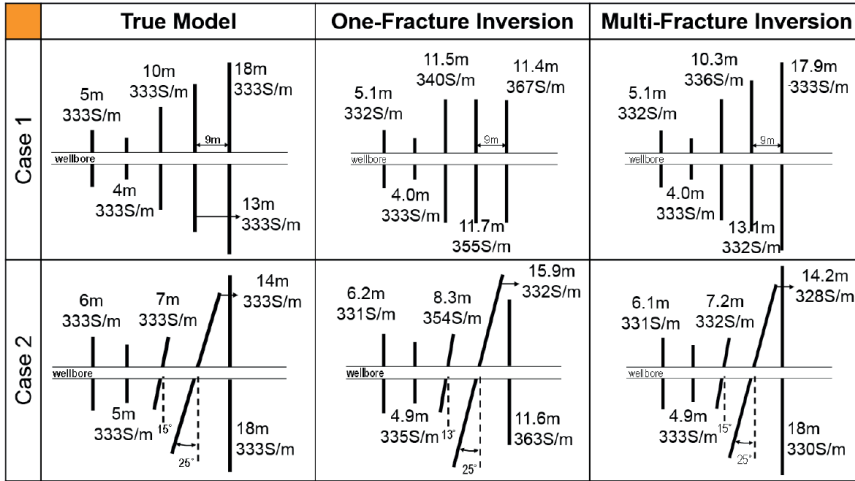


*Figure 8* – **Multi-fracture inversion analysis: left figure shows the true model; middle and right figures show the best result after single- and multi-fracture inversion, respectively**

**Conclusion.** In this paper, we have developed a simulated-annealing based stochastic inversion algorithm to process tri-axial induction data to estimate the geometry and conductivity of hydraulic fractures. It is shown that this inversion analysis can successfully provide good estimates of fracture length, conductivity and dip-angle. In all cases, good agreement is obtained between the true and estimated fracture parameters suggesting that EM induction logging can be a good candidate for detecting the proppant distribution in hydraulic fractures. The following conclusions are obtained from this study.

By using a mono-axial transmitter coil and tri-axial receiver coils, it is possible to recover the effective properties of hydraulic fractures; two coil configurations (co-axial and cross-polarized) and two coil spacings (short and long) are essential to provide the demonstrated description of fracture geometries and conductivities.

For fractures that are assumed to be circular, parameters such as fracture conductivity and radius were shown to be recovered very accurately. For fractures that are assumed to be elliptical, we recover the effective radius for a circle which has the same area as the ellipse. When the proppant concentration varies radially in a fracture (linearly decreasing conductivities towards the fracture tip), the inverted conductivity value is approximately equal to the average conductivity of the fracture. In all these cases, the fracture dip-angle estimated from the measurements is very close to the "true" value because of the sensitivity of the cross-polarized receiver signals to the fracture dip-angle.

For heterogeneous conductivity rock, an accurate estimate of fracture parameters is obtained only after subtraction of the bucked signals with and without a hydraulic fracture. The bucked signals without a fracture can be large enough to affect the inversion accuracy. This highlights the importance of logging the well before and after fracturing operations.

The tool in its current configuration has the capability of detecting conductive fractures up to 40 m in radius. Further improvement can be obtained by improving the sensitivity of the receivers and increasing the tool spacing. This can be achieved with better coil design or a larger conductivity contrast between the rock and the proppants.

For a tool spacing of 18 m, differential signals for the fracture of interest are affected by two neighboring fractures on each side when 9 m spacing is used for the distance between fractures. To invert the results for multiple fractures in a time efficient manner, five fractures should be included in each forward model run. This approach is shown to provide a very accurate estimation of fracture parameters. Including additional fractures in the forward model and the inversion does not influence the final inversion results. 🌐

## REFERENCES

1  Balan, H.O., A. Gupta, and D.T. Georgi, 2017, Feasibility of predicting long-term shale gas production and EURs based on early-time data: Presented at the SPE Middle East Oil & Gas Show and Conference, doi: 10.2118/183754-MS.

2  Basu, S., and M.M. Sharma, 2014, A new method for fracture diagnostics using low-frequency electromagnetic induction: Presented at the SPE Hydraulic Fracturing Technology Conference, doi: 10.2118/168606-MS.

3  Blyton, C.A.J., D.P. Gala, and M.M. Sharma, 2015, A comprehensive study of proppant transport in a hydraulic fracture: Presented at the SPE Annual Technical Conference and Exhibition, doi: 10.2118/174973-MS.

4  Dai, J., Fang, Y, Zhou, J., and Liu, Q.H., 2018, Analysis of electromagnetic induction for hydraulic fracture diagnostics in open and cased boreholes: IEEE Transactions on Geoscience and Remote Sensing, 56, no. 1, pp. 264-271.

5  Fouskakis, D., and D. Draper, 2002, Stochastic optimization, a review: International Statistical Review, 70, no. 3, 315-349, doi: 10.1111/j.1751-5823.2002.tb00174.x.

6  Gianzero, S., Y. Lin, and S. Su, 1985, A new high-speed hybrid technique for simulation and inversion of resistivity logs: SPE Formation Evaluation, 3, no. 1, 55-61, doi: 10.2118/14189-PA.

7  Hoversten, G.M., M. Commer, E. Haber, and C. Schwarzbach, 2015, Hydro-frac monitoring using ground time-domain electromagnetics: Geophysical Prospecting, 63, 1508-1526, doi: 10.1111/1365-2478.12300.

8  LaBrecque, D., R. Brigham, J. Denison, L. Murdoch, W. Slack, Q.H. Liu, Y. Fang, J. Dai, Y. Hu, Z. Yu, A. Kleinhammes, P. Doyle, Y. Wu, and M. Ahmadian, 2016, Remote imaging of proppants in hydraulic fracture networks using electromagnetic methods: results of small-scale field experiments: Presented at the SPE Hydraulic Fracturing Technology Conference, doi: 10.2118/179170-MS.

9  Li, J., and L.C. Shen, 1993, Vertical eigenstate method for simulation of induction and MWD resistivity sensors: IEEE Transactions on Geoscience and Remote Sensing, 31, no. 2, 399–406, doi: 10.1109/36.214916.

10 Pai, D.M., 1991, Induction log modeling using vertical eigenstates: IEEE Transactions on Geoscience and Remote Sensing, 29, no. 2, 209–213, doi: 10.1109/36.73661.

11 Palisch, T., W. Al-Tailji, L. Bartel, C. Cannan, M. Czapski, and K. Lynch, 2016, Recent advancements in far-field proppant detection: Presented at the SPE Hydraulic Fracturing Technology Conference doi: 10.2118/ 179161-MS.

12 Pardo, D. and Torres-Verdín, C., 2013, Sensitivity analysis for the appraisal of hydrofractures in horizontal wells with borehole resistivity measurements: Geophysics, 78, no. 4, pp. D209-D222.

13  Qian, Z.G., W.C. Chew, and R. Suaya, 2007, Generalized impedance boundary condition for conductor modeling in surface integral equation: IEEE Transactions on Microwave Theory and Techniques, 55, no. 11, doi: 10.1109/TMTT.2007.908678.

14  Rao, S.M., D.R. Wilton, and A.W. Glisson, 1982, Electromagnetic scattering by surfaces of arbitrary shape: IEEE Transactions on Antennas and Propagation, 30, no. 3, doi: 10.1109/TAP.1982.1142818.

15  Sen, M. K., and P. L. Stoffa, 2013, Global optimization methods in geophysical inversion: Cambridge University Press.

16  Sharma, M.M., and R. Manchanda, 2015, The role of induced un-propped (IU) fractures in unconventional oil and gas wells: Presented at the SPE Annual Technical Conference and Exhibition, doi: 10.2118/174946- MS.

17  Shiriyev, J., 2018, A tri-axial electromagnetic induction tool for hydraulic fracture diagnostics: Ph.D. Dissertation, The University of Texas at Austin.

18  Shiriyev, J., Y. Brick, P. Zhang, A.E. Yilmaz, C. Torres-Verdin, M.M. Sharma, T. Hosbach, M.A. Oerkfitz, and J. Gabelmann, 2018, Experiments and simulations of a prototype tri-axial electromagnetic induction logging tool for open-hole hydraulic fracture diagnostics: Geophysics, 83, no. 3, D73-D81, doi: 10.1190/GEO2017-0354.1.

19  Shrivastava, K., and M.M. Sharma, 2018, Proppant transport in complex fracture networks: Presented at the SPE Hydraulic Fracturing Technology Conference and Exhibition, doi: 10.2118/189895-MS.

20  Sookprasong, P.A., R.S. Hurt, and C.C. Gill, 2014, Downhole monitoring of multi-cluster, multi-stage horizontal well fracturing with fiber optic distributed acoustic sensing (DAS) and distributed temperature sensing (DTS): Presented at the International Petroleum Technology Conference, doi: 10.2523/IPTC-17972-MS.

21  Wang, G.L., C. Torres-Verdin, and S. Gianzero, 2009, Fast simulation of tri-axial borehole induction measurements acquired in axially symmetrical and transversely isotropic media: Geophysics, 74, no. 6, E233-E249, doi: 10.1190/1.3261745.

22  Wheaton, B., K. Haustveit, and W. Deeg, 2016, A case study of completion effectiveness in the Eagle Ford Shale using DAS/DTS observations and hydraulic fracture monitoring: Presented at the SPE Hydraulic Fracturing Technology Conference, doi: 10.2118/179149-MS.

23  Yang, K., A.E. Yilmaz, and C. Torres-Verdin, 2016, Efficient 3D parametric inversion of hydraulic fractures with low frequency borehole tri-axial electromagnetic measurements: 86th Annual International Meeting, SEG, Expanded Abstracts, 954-958.

24  Yang, K., A.E. Yilmaz, and C. Torres-Verdin, 2017, A goal oriented framework for rapid integral-equation-based simulation of borehole resistivity measurements of 3D hydraulic fractures: Geophysics, 82, no. 2, pp. D121-D131.

25  Yang, K., Torres-Verdin, C., and Yilmaz, A. E., 2015, Detection and quantification of three-dimensional hydraulic fractures with horizontal borehole resistivity measurements: IEEE Transactions on Geoscience and Remote Sensing (TGRS), 53, no. 8, pp. 4605–4615.

26  Zhang, G.J., G.L. Wang, and H.M. Wang, 1999, Application of novel basis functions in a hybrid method simulation of the response of induction logging in axisymmetrical stratified media: Radio Science, 34, no. 1, 19-26, 10.1029/98RS02767.

27.  Zhang, P., J. Shiriyev, C. Torres-Verdin, M.M. Sharma, Y. Brick, J. Massey, and A.E. Yilmaz, 2016, Fracture diagnostics using a low-frequency electromagnetic induction method: Presented at the 50th US Rock Mechanics/Geomechanics Symposium.

28.  Zhang, P., 2018, Low frequency downhole electrical measurements for mapping proppant distribution in hydraulic fractures in cased-hole wells: Ph.D. Dissertation, The University of Texas at Austin.